AERODYNAMIC MODELING AND ASSESSMENT OF FLAPS FOR HYPERSONIC TRAJECTORY CONTROL OF BLUNT BODIES

BY

JOSE SEPULVEDA

THESIS

Submitted in partial fulfillment of the requirements
for the degree of Master of Science in Aerospace Engineering
in the Graduate College of the
University of Illinois at Urbana-Champaign, 2017

Urbana, Illinois

Adviser:

Assistant Professor Zachary R. Putnam

ABSTRACT

Independently articulated aerodynamic flaps on a blunt-body entry vehicle may provide a feasible alternative to current state-of-the-art bank-angle steering control while introducing additional benefits during entry, descent, and landing. Flaps provide direct control of the vehicle's lift and drag vectors, eliminating the need for a center of gravity offset and enabling a relatively constant vehicle attitude. A near-constant attitude may allow the use of relative navigation sensors and regional-scale science instruments during the hypersonic portion of entry. Direct aerodynamic vector control also enables active regulation of heating and reduces or eliminates the need for a reaction control system in the hypersonic regime.

The Configuration-Based Aerodynamics tool was used to predict the trim angle of attack, trim lift-to-drag ratio, lift coefficients, and drag coefficients for variations in the number of flaps, individual flap configurations, and deployment angles. Aerodynamic data is validated against static trim-tab data from the literature. Results for one flap above the entry vehicle are presented for the hypersonic regime with the angle of attack ranging from -4 degrees to 20 degrees. These results demonstrate the effects of a flap on the aerodynamic performance of an entry vehicle and will inform the development of guidance, navigation, and control systems for various flap configurations on entry vehicles.

TABLE OF CONTENTS

LIST OF SYMBOLS & SCRIPTS

List of Symbols

L	Lift force (N)
D	Drag force (N)
M	Pitching Moment (N m)
C_L	Aerodynamic lift coefficient
C_D	Aerodynamic drag coefficient
C_M	Pitching moment coefficient
L/D	In-plane lift-to-drag ratio
σ	Bank angle (deg)
θ	Flap deflection angle (deg)
α	Angle of attack (deg)
β	Ballistic coefficient (kg/m^2)
S	Aerodynamic reference area (m^2)
c	Aerodynamic chord length (m)

q	Dynamic pressure (N/m^2)
ρ	Atmospheric density (kg/m^3)

CHAPTER 1: INTRODUCTION

Landing accuracy for planetary entry, descent, and landing (EDL) systems depends on the accuracy of the approach navigation, day-of-flight uncertainty in the planet's atmosphere, and vehicle aerodynamics. An unguided descent typically corresponds to a larger landing ellipse. For example, Mars Pathfinder and the Mars Exploration Rovers used unguided ballistic entry profiles resulting in landing ellipses of 299 km x 45 km and 70 km x 5 km, respectively [1]. Active trajectory control during hypersonic flight improves landing accuracy. The successful landing of the Mars Science Laboratory (MSL), using the first actively guided planetary entry system, defined a new standard in precision landing technologies [2]. Its guidance system provided a landing ellipse of approximately 20 x 7 km using a modified version of the Apollo guidance algorithm with a reference trajectory [3]. The MSL bank-angle steering trajectory control system represents the current state of the art for EDL systems used at Mars and Earth.

1.1 Bank-angle Modulation

Bank-angle modulation, also known as bank-angle steering, modifies the orientation of an entry vehicle with a non-zero lift-to-drag ratio (L/D) in order to control the direction of its lift vector. Bank angle is the angle between the lift vector and the local vertical. Controlling a vehicle's bank angle changes a vehicle's trajectory by modifying the magnitude of its vertical lift [4], allowing it to satisfy trajectory constraints, such as downrange distance or peak heating. An entry vehicle performs attitude maneuvers to modify the bank angle via reaction control system (RCS) thrusters located around the vehicle.

A vehicle at a nonzero bank angle travels in a crossrange direction due to the lift vector's out-of-plane component. Figure 1 illustrates the in-plane and out-of-plane components of the lift vector. In the figure, the wind-relative velocity vector is pointing directly out of the page.

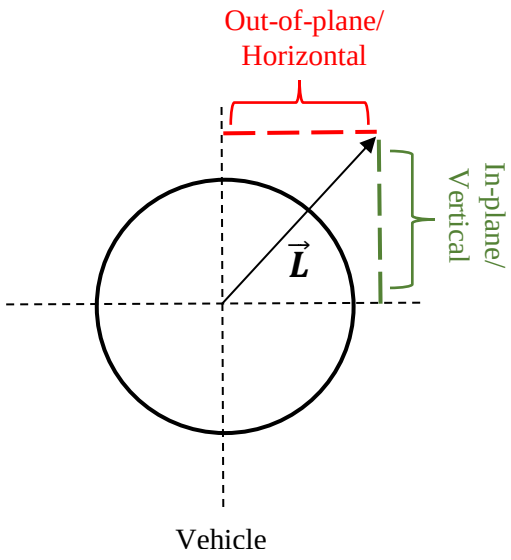

Figure 1: Components of Entry Vehicles' Lift Vector

A bank reversal rotates the vehicle from its current bank angle, assuming the bank angle to be a value other than full lift-up at 0 degrees or full lift-down at 180 degrees, to the same angle with an opposite sign; periodic bank reversals are used to manage crossrange error during entry. Figure 2 depicts a bank reversal maneuver, where changing the bank angle rotates the vehicle's lift about the vehicle's wind-relative velocity vector pointing directly out of the page.

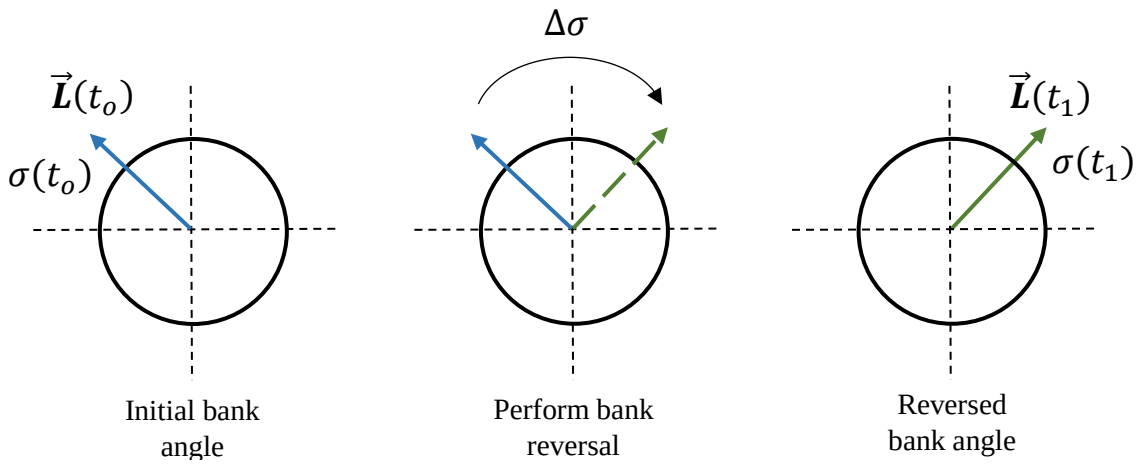

Figure 2: Example of a Bank Reversal Maneuver

However, during reversals, the finite-time lift vector rotation generates steering errors [5]. The in-plane lift-to-drag ratio depends on the cosine of the bank angle, or the vertical component of the lift vector. By modifying, the direction of the lift vector, but not the magnitude, then the value of the in-plane L/D remains constant before and after a bank reversal.

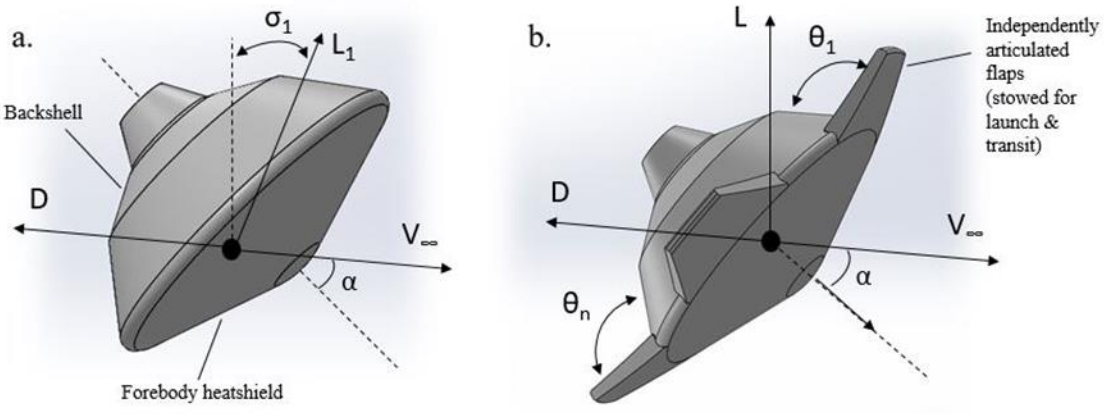

Figure 3. (a) MSL-like Entry Vehicle Identifying Bank Angle, σ1 (b) MSL-like Entry Vehicle with a Four-Flap Configuration Identifying Total Angle of Attack, α.

Figure 3 shows a comparison between bank-angle modulation (a) and independently articulated flaps (b). Figure 3a shows the bank angle, σ_1, with respect to the local vertical. In this diagram, a bank angle change rotates the lift vector out of or into the page. Figure 3b depicts a conceptual four-flap design on an MSL-like entry vehicle. Each flap is capable of stowing along the backshell for launch. The flaps are deployed prior to entry interface. Changes in the angle of each flap may be used to modify total angle of attack, α, and sideslip angle. Since multiple flap configurations may be used to produce a desired angle of attack, the flaps may be set to achieve both the desired angle of attack, and therefore L/D, as well as satisfy other mission parameters and constraints, such as peak heat rate limits.

1.2 Aerodynamic Flaps

Independently articulated aerodynamic flaps modify a blunt-body entry vehicle's drag area and angle of attack as each flap's deployment angle changes. This provides direct control of the lift and drag vectors, potentially allowing an entry vehicle to maintain a near-constant attitude during EDL. Independent articulation of the flaps adjusts the attitude of an entry vehicle although the quantity of flaps may define the required deployment angles. A minimum of two flaps are required for control of total angle of attack. For example, a vehicle with one flap would only be capable of modifying its angle of attack because of the orthogonality of the sideslip angle. Any vehicle with more than one flap may control its angle of attack and sideslip angles, provided the flaps are not located 180 degrees from each other. The advantage of increasing the number of flaps is the freedom to select other parameters. As an example, a vehicle with four small flaps as opposed to two larger flaps is capable of producing the same angle of attack and sideslip values while also deploying its flaps at angles that decrease its ballistic coefficient, β. A vehicle with a lower ballistic

coefficient experiences more drag deceleration at higher altitudes, improving descent timeline and margin for entry at Mars [6].

1.3 Background

Aerodynamic flaps for trajectory control have not been extensively studied in the past. Previous studies of aerodynamic flaps consist predominantly of a single flap or static trim tabs. A single trim flap was evaluated for several projects, such as the Space Shuttle, Mars Surveyor, and a lunar return capsule. Hypersonic wind tunnel data and Navier-Stokes computational predictions for Mars Surveyor showed that a single flap could deliver sufficient trim to provide similar aerodynamic performance as offsetting the vehicle's center of gravity [7]. The use of a trim flap on the Crew Exploration Vehicle (CEV) Orion was assessed with first-order engineering design tools based on incidence angle methods and CFD methods [8]. Results from both methods showed an increase in the trim L/D from roughly 0.26 to 0.305 using a flap of one square meter in surface area [8]. An increase in L/D also increases the available cross-range, which is beneficial for the selection of landing sites.

A recent study on entry body control flaps uses a two-body-flap control system onboard ESA's Intermediate Experimental Vehicle [9]. The lifting-body vehicle launched on February 11, 2015 as a testbed to validate various re-entry technologies, including a two-flap control system [9]. The system controls the vehicle's pitch and roll using different deflections via electromechanical actuators on each flap. The complex aerothermodynamic processes caused by the generation of shock waves from the flaps' motion were surveyed by 21 thermocouples, 4 pressure sensors, and an infrared (IR) camera. The IR camera also obtained thermal evolution data on the flaps, while thermocouples and pressure sensors observed the aerothermodynamics between the flap hinge and

the hinge TPS [9]. Flight performance data showed that the vehicle does not require the use of RCS during entry [9].

Trim tabs are deployable surfaces on an entry vehicle allowing it to modify its aerodynamic performance parameters, including its L/D. The tabs typically extrude from the heatshield, or near it, into the flow and remain stationary once deployed. NASA Langley Research Center examined 38 different trim tab configurations for supersonic blunt-body entry vehicles using a hypersonic wind tunnel. Each model configuration consisted of a different model shape or a different trim tab angle relative to the local vertical. The experiments altered the vehicle's angle of attack to observe aerodynamic performance changes at a maximum airflow velocity of Mach 4.5. This assessment concluded that trim tabs are a viable approach to improve the aerodynamic performance of blunt-body entry vehicles [10].

1.4 Potential Benefits and Costs of Flaps

The addition of flaps on an entry vehicle may provide several in-flight benefits over bank-angle modulation. First, the use of the RCS may be significantly reduced or eliminated during hypersonic flight. The reduction in RCS thruster usage mitigates RCS-jet-wake flow interaction effects and reduces the required propellant mass, at an added cost of the mass of the flaps and actuation system. The flaps maintain direct control of the lift vector allowing an entry vehicle to maintain a relatively constant attitude, eliminating bank-angle reversals and their associated transients. Flaps may also enable use of navigation and science instruments during descent. These benefits must be assessed relative to costs, including technology development risk, potential increased system mass, and increased complexity.

1.4.1 Potential Benefits of Flaps

An entry vehicle using flaps would significantly reduce or eliminate RCS usage during hypersonic flight. Similar hypersonic entry trajectories can be flown by adjusting a vehicle's vertical lift using flaps as with banking maneuvers. The reduction in RCS thruster usage minimizes uncertainties in the aftbody airflow and possibly allows propellant mass to be redistributed as payload mass. RCS jet flows mix with the airflow around the vehicle generating complex interaction effects. These effects may alter the aerodynamic characteristics as well as the aerothermodynamic environment of the vehicle's backshell [11]. For example, Apollo Program experiments showed that the capsule's roll and yaw jets caused significant interference heating on the Apollo shape while the roll jets also produced a moment due to increased pressure [11]. Similarly, MSL experienced significant RCS-aerodynamic interactions using its initial thruster orientations although the final design had low to moderate interference effects [11]. Accurate modeling of interaction effects requires Computational Fluid Dynamics (CFD) and wind tunnel testing. These interaction effects are not well understood, creating a problem for the CFD software. The most accurate data would result from expensive wind tunnel or flight-testing. Furthermore, the use of RCS thrusters for bank-angle reversals rotates the lift vector as the bank angle changes to its new value. The rotation takes on the order of 10s of seconds, during which the vector is oriented in the wrong direction during the reversal. Bank reversals, although required for bank-angle steering systems, reduce trajectory control authority and margin.

Radar sensors can collect terrain-matching data to enhance landing precision and accuracy. The use of radar altimeters and Doppler radar during EDL has been well documented for previous Mars missions, although rarely in the hypersonic regime. The Mars Viking mission used a radar altimeter during its hypersonic descent stage, resulting in an improved landing accuracy [12]. The

altimeter began recording data at 132 km while Doppler radar began at 5 km; both sensors recorded data until landing [12]. During the terminal descent stage, Mars Pathfinder (MPF), Mars Exploration Rovers (MER), Phoenix, and MSL have all used radar altimeters [13]. MPF used a radar altimeter during descent for the final 1591 m, after heatshield separation [14]. This allowed the onboard flight software to calculate when to activate certain systems, such as airbag inflation [14]. An entry vehicle with a constant attitude would be capable of using radar throughout the EDL sequence because it would remain focused toward the landing site. This would also reduce the risk of altitude errors caused by large terrain features. Hills, trenches, and surface slopes can essentially "spoof" Doppler radar and radar altimeters [13]. The low altitude at which radar is typically activated in the terminal descent stage affects the efficiency of radar instruments.

A constant attitude entry vehicle would also be capable of maintaining high-bandwidth communication with Earth or orbital assets, since its backshell orientation would be known. MPF experienced issues with its low-gain, omnidirectional communication system during EDL due to ionized particles [15]. The spacecraft used a backshell low-gain antenna to communicate with Earth and experienced a 30-second blackout [15]. High-gain antennas can send and receive data at higher rates, but are more susceptible to loss of signal. The antennas capture a greater portion of a received signal if they are accurately pointed at the incoming signal [16]. A vehicle with aerodynamic flaps entering an atmosphere would contain the attitude accuracy required to use a high-gain antenna rather than multiple lower gain antennas during descent. This would allow for receivers on Earth to capture more of the signal at a higher rate than if low-gain antennas were used, and potentially allow navigation information to be sent to the vehicle during descent from orbital assets.

1.4.2 Potential Hypersonic Science Platform

By maintaining a constant attitude during descent, a vehicle can serve as a scientific platform to gather new data in an unexplored regime. Any entry vehicle traversing through a planet's atmosphere is capable of providing in-situ or remote measurements unobtainable via satellites or landers [17]. The vehicle can serve as an alternative to the currently proposed Preliminary Research Aerodynamic Design to Land on Mars (Prandtl-m) airplane and the Aerial Regional-scale Environmental Survey (ARES) airplane concept [18]. Aerial platforms may provide crucial information to advance our understanding of planets and celestial bodies with an atmosphere. For example, Mars' lower atmosphere is difficult to observe from orbit although it changes drastically with latitude due to chemical processes, surface processes, and transport [17]. A large section of this regime can be explored with mass spectrometers, radiometers, and cameras onboard an entry vehicle during descent rather than from a lander confined to a comparatively small region on the ground. These instruments could aid in understanding the processes and history of Mars' climate [19]. The entry vehicle's constant attitude would also allow radar sensors to detect landing sites and improve landing accuracy. Using Mars as an example, the vehicle would be capable of identifying landing hazards less than a meter in diameter, which is the resolution of the High Resolution Imaging Science Experiment (HiRISE) camera onboard Mars Reconnaissance Orbiter (MRO) [20]. Entry vehicles with active guidance and radar sensors would help reduce the risk involved in landing a surface probe by tracking and avoiding potential hazards.

1.4.3 Aerodynamic Flap Concept Costs and Unknowns

Aerodynamic flaps contain potential costs due to their technology investment and currently unknown performance parameters during flight. This study aims to begin developing performance

parameters for various configurations of flaps during hypersonic and supersonic entry phases. Currently, these performance parameters are being investigated via low fidelity simulations. The most significant performance issue may concern the vehicle's dynamics, including the ability to control roll, which may result in additional requirements on the development of flap deployment mechanisms. The RCS thrusters are capable of controlling this rotation, but it is unknown how different flap configurations will be able to support this function. The configuration and number of flaps could significantly alter the vehicle's dynamics, resulting in more testing to model accurate in-flight behavior. The deployment, or deflection, angle of each flap will also affect the vehicle's attitude. This angle would depend on the quantity, location, and size of each flap. Since the flaps are stowed during launch and not activated until the EDL phase, a reliable deployment system is required to perform necessary modifications. The actuation system must also rotate the flaps relatively quick to perform required angle of attack modifications while providing sufficient torque to counter hypersonic aerodynamic forces. Their ability to implement alpha and beta, or total angle of attack, control will require detailed analyses. Hinge, actuation, and deployment failures are also critical issues requiring further analyses. The vehicle's thermal protection system (TPS) will also require examination, particularly at the hinges, to avoid airflow through the heatshield. The material properties for the flaps need to be investigated to ensure that deflections, heat rates, and other issues can be tolerated. The material choice will also affect the mass of the system. The flaps will be assessed relative to bank-angle modulation in terms of subsystem mass, complexity, impact on subsystems, and flight performance.

CHAPTER 2: METHODOLOGY

The analyses for determining the aerodynamic parameters of various flap configurations on entry vehicles requires several steps for pre-processing, simulating, and post-processing the data. While several entry vehicle designs have been considered in previous experiments, only one sphere-cone model was selected for these flap configurations. During pre-processing, the first step is to develop a CAD model for the selected entry vehicle. For this assessment, SolidWorks was selected due to its accessibility and user-friendly interface. The entry vehicle CAD model is saved as its own entity in order to examine its aerodynamic effects. After model development, the desired flap, or assembly of flaps, are defined at a deflection angle. Each flap is modeled as its own CAD part and then mated onto the entry vehicle to form an assembly. The overall assembly, with proper coordinate axes, is saved as a STEP file. Using the Gmsh software, a two–dimensional mesh can be superposed on the three-dimensional model surface. The created mesh forms triangular sections with the selected nodal points. This mesh is refined by splitting each section, hence increasing the total nodal points, for more precise data acquisition during the simulation. The meshed model is saved as a .mail file, which can be converted into an msh file using a script in MATLAB. The script modifies the organization of the saved mesh nodal points to align with the required format. The mesh file is used as the primary input into the Configuration-Based Aerodynamics (CB Aero) software. The following figure depicts a flowchart of the required steps in order to calculate the aerodynamic parameters of an entry vehicle with one or more flaps.

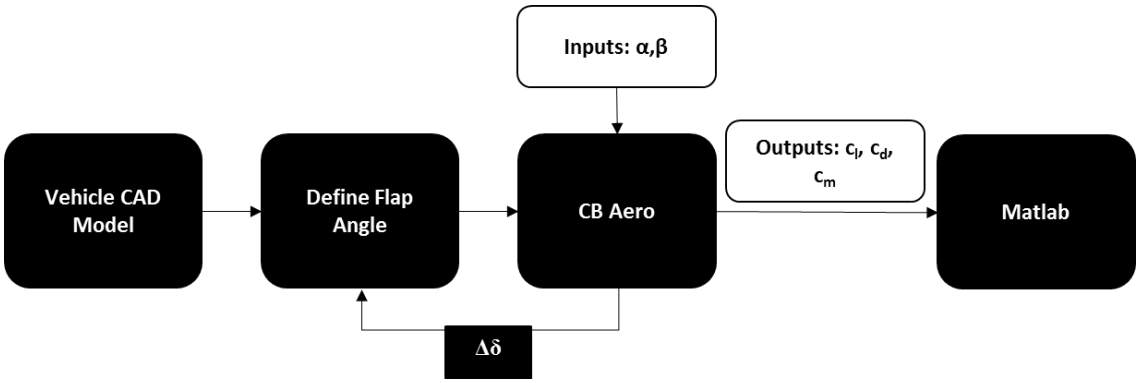

Figure 4: Process for Calculating Aerodynamic Parameters

The CB Aero simulation uses the total angle of attack, or α and sideslip values corresponding to the in-plane and out-of-plane angles, as inputs to define the orientation in which the vehicle will rotate. This software creates its own text file listing all of the required input parameters. A new simulation is required for each change in flap deflection angle since the flap is assembled to the vehicle on the CAD software and not in the simulation. The aerodynamic coefficients and forces outputted are all saved to text files. During post-processing, these files are imported into MATLAB to determine the desired aerodynamic effects for a particular vehicle geometry. The original entry vehicle model is also simulated in order to determine the individual contribution of each flap to the overall vehicle aerodynamics.

2.1 Configuration-Based Aerodynamics (CB Aero) Method

CB Aero uses a Modified-Newtonian independent panel method to calculate the surface pressure at each triangular mesh point. These values are used to determine the overall lift coefficient, drag coefficient, pitching moment coefficient and lift-to-drag ratio for variations in flap configurations and flap deployment angles. The vehicle geometry is derived from the imported mesh file, which is initially setup to specify the solver settings. An input file is created during this setup to define

the angles of attack, sideslip angles, Mach number, dynamic pressure, planetary atmosphere, and location of the center of gravity (C.G.) for the vehicle. By default, the output will be all aerodynamic parameters and heating parameters. Since no thermal protection system was defined for this assessment, the heating data was combined with the flow streamlines only to verify whether the flap was accurately located on the vehicle. Figure 5 displays an image of a model with surface heating and flow streamlines overlaid on the vehicle to verify a proper angle of attack for a top flap geometry.

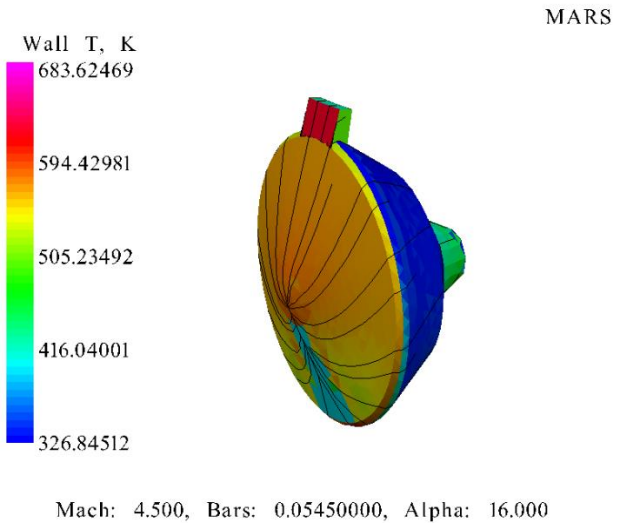

Figure 5: CB Aero Diagram of Heating and Flow Streamlines

2.2 CB Aero Parameters

CB Aero requires multiple parameters input into the setup file, as listed above. These parameters depend on the entry vehicle, flap placement, and desired entry conditions at a selected planet. Although the input file requires a Mach number and corresponding dynamic pressure, a planet must also be selected from a drop-down list. For these simulations, data was acquired during the

hypersonic and supersonic regime of a Martian descent. All data presented in this assessment assumed an EDL sequence on Mars with simulated atmospheric conditions.

2.2.1 Mars Planetary Data

The Martian atmospheric model was derived from the selection of "MARS" on the input file. CB Aero calculates the speed of sound based on free stream conditions in temperature, ratio of specific heats, and gas constant. The 1976 standard atmospheric model is used for Earth, while a similar model is selected for other planets [21]. The user-given Mach numbers and dynamic pressures are combined with an atmospheric model to determine the free stream conditions, altitude, and velocity of the entry vehicle. The following data in Table 1 was selected as the flight conditions for different simulations. The Mach numbers and corresponding dynamic pressures were derived from a three degree-of-freedom simulation using a Mars Phoenix entry trajectory. While atmospheric data may vary depending on conditions, an aerodynamic database for the Mars Phoenix entry capsule was constructed using continuum flow-field computations and EDL data from previous Mars rover missions [22]. The comprehensive database also contains hypersonic and supersonic static coefficients with sensitivities to atmospheric density within uncertainty bounds [22]. This data was used to form a simulated entry trajectory, from which the values in Table 1 were interpolated for use in these CB Aero simulations.

Table 1: Mars Parameters

Simulation Case	Mach Number	Dynamic Pressure (bars)
1	4.5	0.0367
2	20.0	0.0742

2.2.2 Entry Vehicle Parameters

The vehicle selected for all simulations was an MSL-like entry capsule with a 70-degree sphere-cone. This model was chosen due to its publicly available reference geometry in order to reconstruct it as a CAD model. The previously described trim tab experiments by NASA Langley also included a 70-degree sphere-cone shroud for which an initial CB Aero simulation can be validated. Table 2 displays the selected parameters for the sphere-cone vehicle used in all simulations. The center of gravity vector is referenced from the origin of the coordinate axes defined by the vehicle CAD model. The model was sketched with the purpose of placing the center of gravity at the origin to prevent a required offset in the simulations. These values correspond to the base vehicle whereas the parameters for each flap are given in later sections depending on the simulation case.

Table 2: Entry Vehicle Parameters

Parameter	Value for 70° Sphere-Cone
Aerodynamic surface area (m^2)	15.9043
Diameter (m)	4.5
Nose radius (m)	1
Center of Gravity ([X,Y,Z])	[0,0,0]

The final input requirements for a CB Aero simulation include the flight parameters for the entry vehicle. Table 3 depicts the ranges for angle of attack and sideslip angle, or the in-plane and out-of-plane components of the vehicle's total angle of attack, respectively. In these simulations, the sideslip angle was maintained constant so that only in-plane angle changes were investigated.

Table 3: Flight Parameters

Parameter	Value for 70° Sphere-Cone
Angle of Attack (deg)	-4 to 20
Sideslip Angle (deg)	0

2.3 Limitations of CB Aero

Although CB Aero is able to produce low-fidelity aerodynamic data, it does have some restrictions. If each flap is considered as a control surface, then it uses superposition to determine flap effects. Thus, it uses aerodynamic parameter changes in each flap separately and sums the changes to produce final parameters for each configuration. This method does not account for interaction effects if more than one flap exists. The predefined "CB Defs" function in the software uses the vehicle's characteristics to determine aerodynamic parameters for a given flap configuration, but also ignores interaction effects using superposition. Overall, the accuracy is improved by inputting a new model for every flap configuration and running each case as its own simulation.

2.4 MATLAB Post-Processing

The post-processing stage utilized MATLAB codes to determine the lift coefficient, drag coefficient, pitching moment coefficient and lift-to-drag ratio for any desired flap angle and size. If more than one flap is present, superposition is implemented to determine the effect of each flap on the entry vehicle. Data from the vehicle without flaps and the vehicle with one flap in a desired

location is read into a function to distinguish the flap's effects. Each flap's contribution effects are summed with the vehicle's aerodynamic parameters to determine the overall aerodynamic performance for this vehicle configuration. The function that calculates the aerodynamic coefficients is called by a separate script used to compute and plot the trim conditions for this vehicle configuration. The input for the MATLAB functions are the vehicle's force and moment vectors to output the aerodynamic coefficients and trim conditions. Figure 6 displays the coordinate axes defined by CB Aero for the text files used in the MATLAB functions.

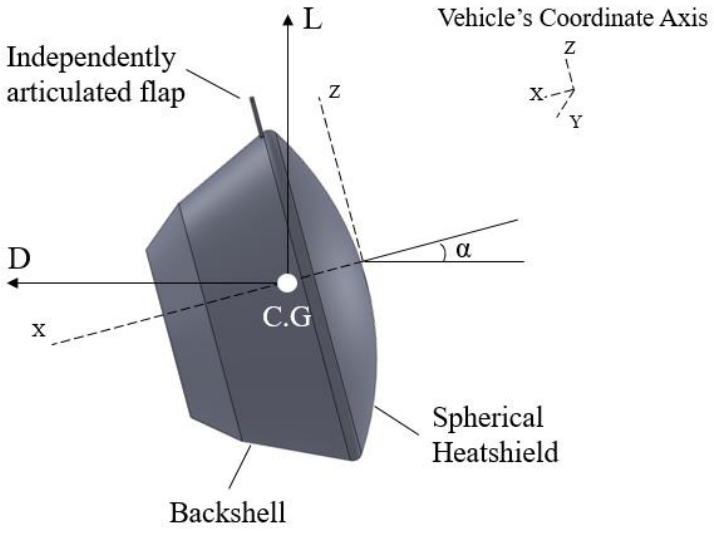

Figure 6: Diagram of Vehicle's Coordinate Axes Defined by CB Aero

The MATLAB function used to calculate the lift, drag, and pitching moment coefficients initially reads the aerodynamic force coefficients on the vehicle as the input. These force coefficients are in three separate files based on their axis component. Equation 1 depicts the notation of the aerodynamic force coefficient in terms of its component form.

$$\boldsymbol{C_F} = [C_{F_X}, C_{F_Y}, C_{F_Z}] \tag{1}$$

The force coefficient must be made into vector format so that a flap rotation can be achieved if necessary for a desired geometry. Equation 2 illustrates the equation for an aerodynamic force vector in terms of its aerodynamic coefficients.

$$\boldsymbol{F} = \frac{1}{2}\rho v^2 A \boldsymbol{c_F} = qS\boldsymbol{c_F} \tag{2}$$

Equation 2 contains the aerodynamic force vector to compute the drag and lift vectors. If a rotation is necessary, then the force vector is multiplied by a rotation matrix. However, if no rotation is necessary then the next step depends on how many flaps are desired. For a one-flap configuration at a given angle of attack, the resulting force vector in Equation 2 can be decomposed back into component form and then used to solve for the coefficients of lift and drag, as given by Equations 3 and 4, respectively.

$$C_L = C_{F_Z} * \cos\alpha - C_{F_X} * \sin\alpha \tag{3}$$

$$C_D = C_{F_X} * \cos\alpha + C_{F_Z} * \sin\alpha \tag{4}$$

If a two-flap configuration is desired, then the contribution of each flap must be assessed. Equation 2 is defined for each flap case and the no flap case, resulting in three different force vectors for the vehicle with one top flap, one bottom flap, and no flaps. The contribution of each flap is calculated by subtracting the general vehicle's aerodynamic vector from the force vector of the vehicle with one flap. Equation 5 illustrates this difference.

$$\boldsymbol{dF}_{top/bot} = \boldsymbol{F}_{top/bot} - \boldsymbol{F}_{no\ flaps} \tag{5}$$

Calculating Equation 5 for both the top and bottom flap contributions, the total aerodynamic force vector can be determined using superposition, as shown by Equation 6.

$$\boldsymbol{F}_{total} = \boldsymbol{F}_{no\ flaps} + \boldsymbol{dF}_{top} + \boldsymbol{dF}_{bot} \tag{6}$$

The aerodynamic force coefficient can be determined from Equation 2 using this new total force. Equations 3 and 4 can then be applied to solve for the lift and drag coefficients.

The MATLAB function also reads separate files for the moment vector coefficients, similar to the aerodynamic force coefficients. The component form of the moment vector is given as follows by Equation 7.

$$\boldsymbol{C_M} = [C_{M_X}, C_{M_Y}, C_{M_Z}] \tag{7}$$

By the same reasoning as the aerodynamic force vector, the moment vector must also be explicitly written from its coefficient. The moment vector has units of N m and is defined by Equation 8.

$$\boldsymbol{M} = \frac{1}{2}\rho v^2 cA\boldsymbol{c_M} = qcS\boldsymbol{c_M} \tag{8}$$

Similar to the aerodynamic force vector, if a rotation is necessary, then the moment vector is multiplied by a rotation matrix. For a one-flap configuration at a given angle of attack, the moment vector from Equation 8 can be solved back into component form and then used to solve for the pitching moment coefficient using Equation 9.

$$C_M = C_{M_Y} \tag{9}$$

For a two-flap configuration, the same process as with the aerodynamic force vector is followed to obtain the contribution of each flap, resulting in Equations 10 and 11.

$$\boldsymbol{dM}_{top/bot} = \boldsymbol{M}_{top/bot} - \boldsymbol{M}_{no\ flaps} \tag{10}$$

$$\boldsymbol{M}_{total} = \boldsymbol{M}_{no\ flaps} + \boldsymbol{dM}_{top} + \boldsymbol{dM}_{bot} \tag{11}$$

Equation 6 can then be decomposed to solve for the moment coefficient using Equation 8. As before, the pitching moment coefficient is the value of Equation 8 in the y-direction and is given by Equation 9.

The MATLAB function used to calculate the vehicle's trim conditions calls a script with the above equations for each angle of attack in the simulation. Once the aerodynamic coefficients have been determined and placed into an array, the trim condition may be found by interpolating the pitching moment coefficient array to solve for when it crosses zero. This is the trim angle of attack. Using this value, the index of the array may be found and used to calculate the trim c_l, c_d, and L/D at the same angle of attack value.

CHAPTER 3: VALIDATION WITH TRIM TAB DATA

Previously, there has not been a variety of experimental data produced for trim tabs or flaps on planetary entry vehicles. One recent and comprehensive analysis was performed by NASA Langley using 38 hypersonic wind tunnel experiments [10]. From the resulting data, one entry vehicle model was selected as a validation case to compare the accuracy of using CB Aero for further analyses. The model selected for CB Aero was an MSL-like entry capsule with a 70-degree sphere-cone analogous to the shroud used by Langley. The Langley model was six inches in diameter and the trim tab had a zero-degree cant angle relative to the heat shield. A cant angle is the angle created by the trim tab relative to the heat shield angle. For example, a trim tab flush with the heat shield would have a zero-degree cant angle. This model used a trim tab of 3% relative to the base area. The parameters for the simulation model are defined in the next section. The purpose of this validation case was to verify whether the low-fidelity CB Aero software could produce similar results to experimental wind tunnel data. Figure 7 displays the shroud model used in the wind tunnel experiments at NASA Langley.

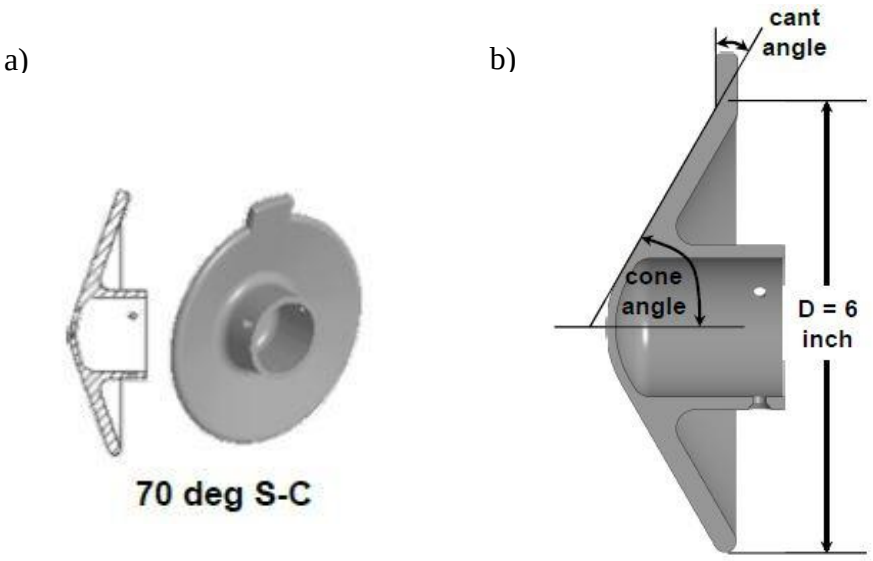

Figure 7: (a) Rear View of 70-Degree Sphere-Cone Shroud with 3% Trim Tab and (b) Side View of 70-Degree Sphere-Cone Shroud with 3% Trim Tab at a 20-Degree Cant Angle

3.1 Sphere-Cone Model

The model used in the CB Aero simulations was a 70-degree sphere-cone with the backshell modeled after the MSL entry capsule. The 70-degree sphere-cone shroud was selected as the validation case because it could be compared to an existing entry capsule for which the dimensions were obtained through publications. The wind tunnel and simulation models contained the same relative dimensions with the only difference between the two models being the existence of a backshell in the simulation case. Figure 8 displays the simulation CAD model with a trim tab of 3%, created to ensure that all parameters remained the same as in the wind tunnel experiment.

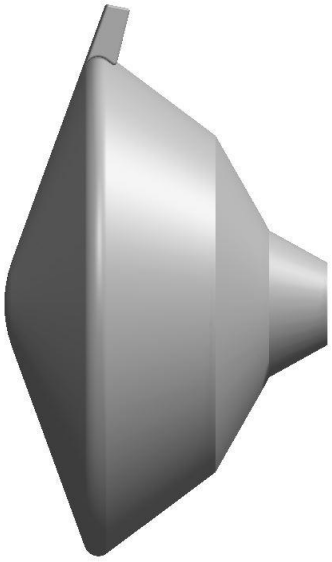

Figure 8: Side View of 70-Degree Sphere-Cone Model with a 3% Trim Tab at 0-Degree Cant Angle

3.2 Comparison of Aerodynamic Parameters

The following plots compare the results obtained from the CB Aero simulations with the NASA Langley wind tunnel data at Mach 4.5. The tab in both cases was 3% of the base area, had a 2:1 tab width to height ratio, and was at a 0-degree cant angle. The angles of attack examined were from -4 degrees to 20 degrees increasing in 2-degree increments. All data for the wind tunnel experiments was extrapolated from the resulting plots from [10] since the numerical data was unavailable. Figure 9 shows the coefficient of drag as a function of angle of attack for both models. While the difference appears large, that is due to the scaling of the y-axis. The difference is less than 8 percent at the maximum error near 0-degree angle of attack.

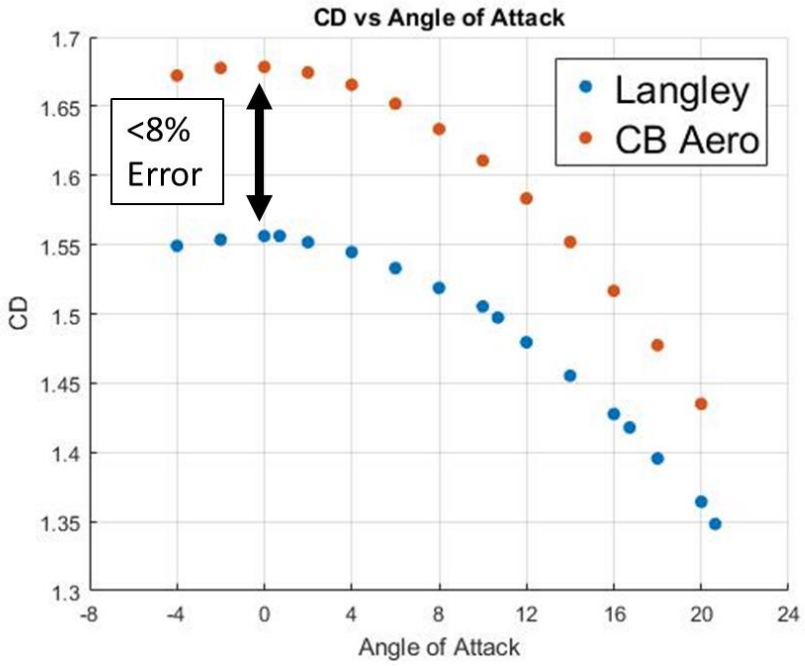

Figure 9: Comparison of Drag Coefficient vs Angle of Attack

The following Figure 10 displays the coefficient of lift as a function of angle of attack for both models with the 3% trim tab. The data aligns very well with a difference of less than one percent. The points do not align exactly due to the angle of attack being defined by integer values in the simulation but only approximated in the wind tunnel experiments.

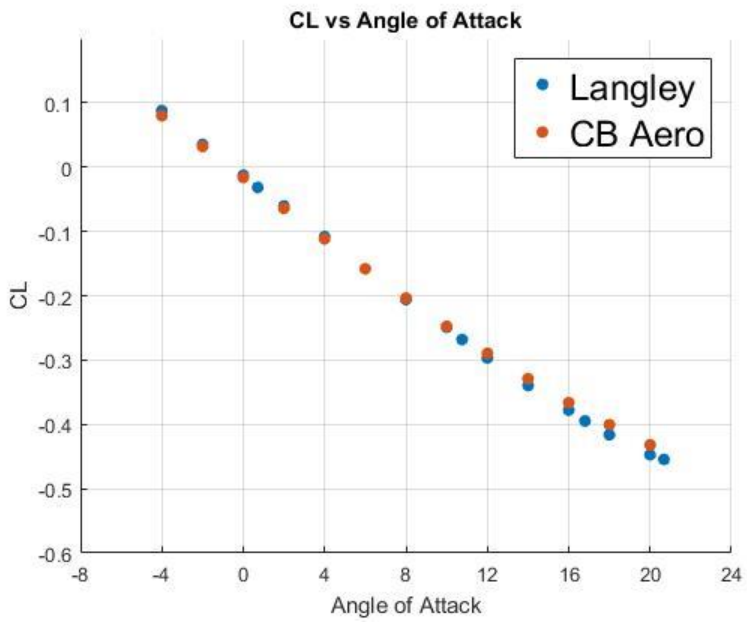

Figure 10: Comparison of Lift Coefficient vs Angle of Attack

The following Figure 11 displays the pitching moment coefficient as a function of angle of attack for both vehicle models. The trim angle of attack is defined as the angle at which the vehicle has no pitching moment so c_m is zero. Using this plot and interpolating the data, the trim angle of attack for the CB Aero simulation is found to be 8.95 degrees. The wind tunnel data produced a trim angle of attack of 8.846 degrees. The error between the two values is 1.2 percent meaning that the data matches well. In this case, CB Aero performs comparatively to wind tunnel experiments.

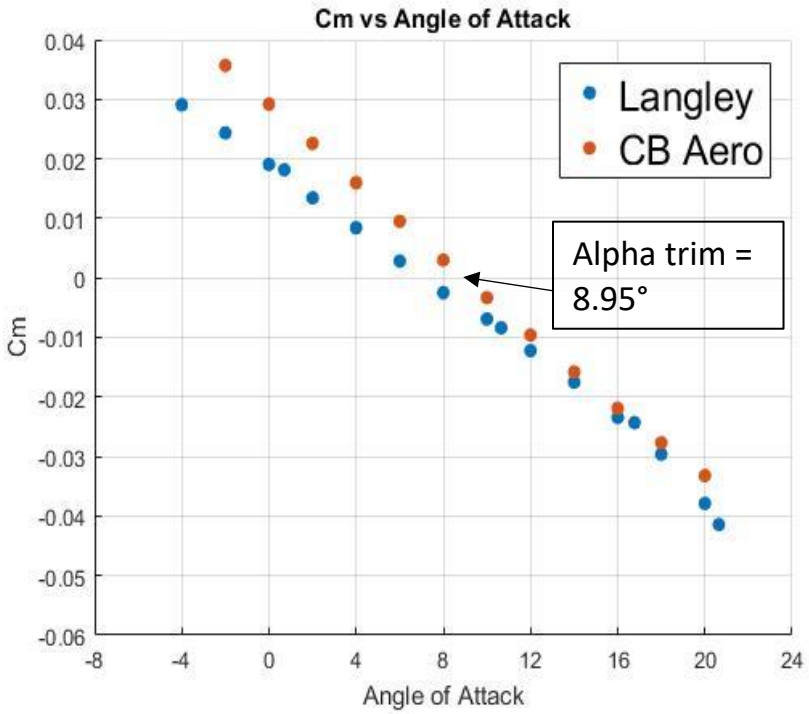

Figure 11: Comparison of Pitching Moment Coefficient vs Angle of Attack

The following Figure 12 shows the lift-to-drag ratio, or L/D, as a function of angle of attack for both of the models. The trim lift-to-drag ratio is defined as the value at which the vehicle is trimmed, or has no pitching moment. This is calculated by using this plot at the trim angle of attack. The trim L/D was interpolated from the data and found to be -0.138 for the CB Aero simulation. The wind tunnel data resulted in a trim L/D of -0.149. The error between these values is 7.4 percent, meaning that the simulation is acceptable.

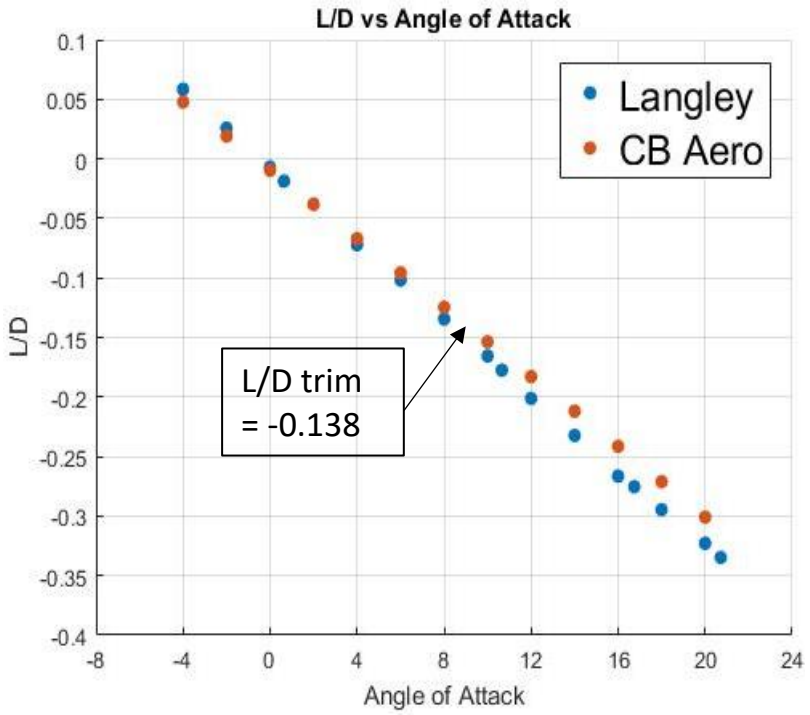

Figure 12: Comparison of Lift-to-Drag Ratio vs Angle of Attack

The trim conditions produced by this validation case matched within a tolerable value. It was determined that CB Aero can be used to simulate aerodynamic parameters because the validation case results were within 10 percent of the wind tunnel data. This percentage was selected since CB Aero is of low-fidelity and only used to conduct preliminary analyses. With the simulation results validated by this case, more variations of flap configurations may be considered.

CHAPTER 4: AERODYNAMIC PERFORMANCE OF A DEPLOYABLE FLAP

The first analysis for aerodynamic flaps on an entry vehicle involves attaching only one deployable flap. A deployable flap requires analyses conducted at various deflection angles and vehicle angles of attack in order to observe its aerodynamic performance. Single flap effects may be decoupled from the vehicle's aerodynamic parameters at low to mid angles of attack in order to use superposition while ignoring interaction effects. The following Figure 13 shows possible flap configurations for blunt-body entry vehicles, ranging from one to four flaps equally spaced around the vehicle. The results for the first configuration are shown here although post-processing listed the method to analyze results from the first two configurations.

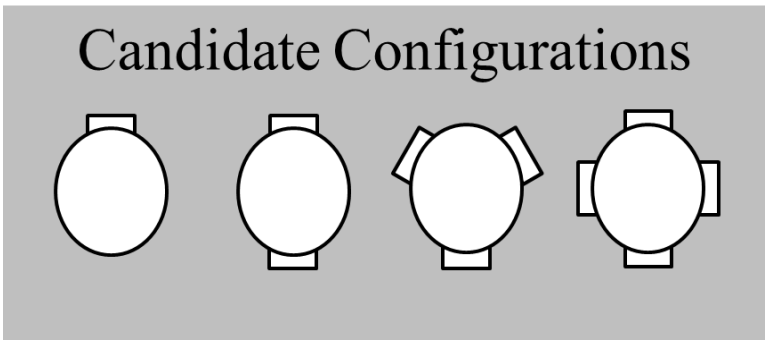

Figure 13: Candidate Flap Configurations for Entry Vehicles

4.1 Seventy Degree Sphere-Cone Model with a Flap

The model used in this simulation was a 70-degree sphere-cone with a 3% flap on top, deflecting from a cant angle of 0 to 40 degrees. These cant angles translate to flap deflection angles of 70 to 30 degrees, respectively. For this simulation, the cant angles were defined as positive for the flap

moving towards the stowed configuration on the backshell. A comparison was conducted in terms of aerodynamic performance parameters, or trim L/D and trim angle of attack. The flap was placed on the heat shield and not behind it in order to make it flush with the rest of the shield. The flow interaction effects at the hinge have not been studied in detail due to the limitations of this simulation, although it is expected that heating will become an important concept to analyze. Figure 14 displays the vehicle model with a 3% flap at a 50-degree deflection angle from the vehicle's body x-axis.

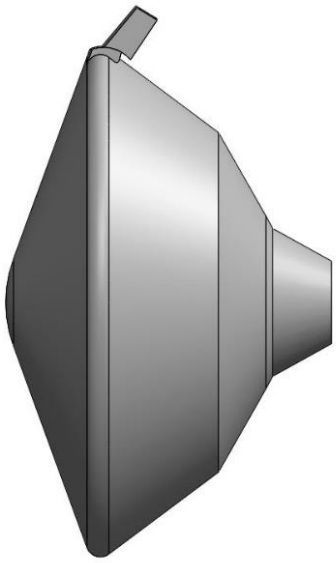

Figure 14: Diagram of 70-Degree Sphere-Cone with a Flap at a 50-Degree Deflection Angle

The flap used in this configuration had a 3% tab area relative to base area, 2:1 tab width to height ratio, and rotated from deflection angles of 30 degrees to 70 degrees, by increments of 10 degrees. This is essentially the same tab used in the validation case but with a deflection angle included to simulate deployment. The simulation parameters for this case included a Mach number of 4.5 and angles of attack ranging from -4 degrees to 20 degrees.

4.2 Aerodynamic Performance Results

This section presents the results for the pitching moment coefficient and trim aerodynamic conditions for each flap, or tab, deflection angle calculated by the MATLAB functions. The 70-degree sphere-cone vehicle with a 3% flap at a 70-degree deflection angle was validated with wind tunnel data in the previous chapter. This section depicts how the aerodynamic parameters are affected by the change in the flap's deflection angle. The pitching moment coefficient is a function of angle of attack and is displayed for each of the five deflection angle cases. The trim conditions are displayed as functions of the flap deflection angle. The following Figure 15 displays the pitching moment coefficients for varying flap deflection angles.

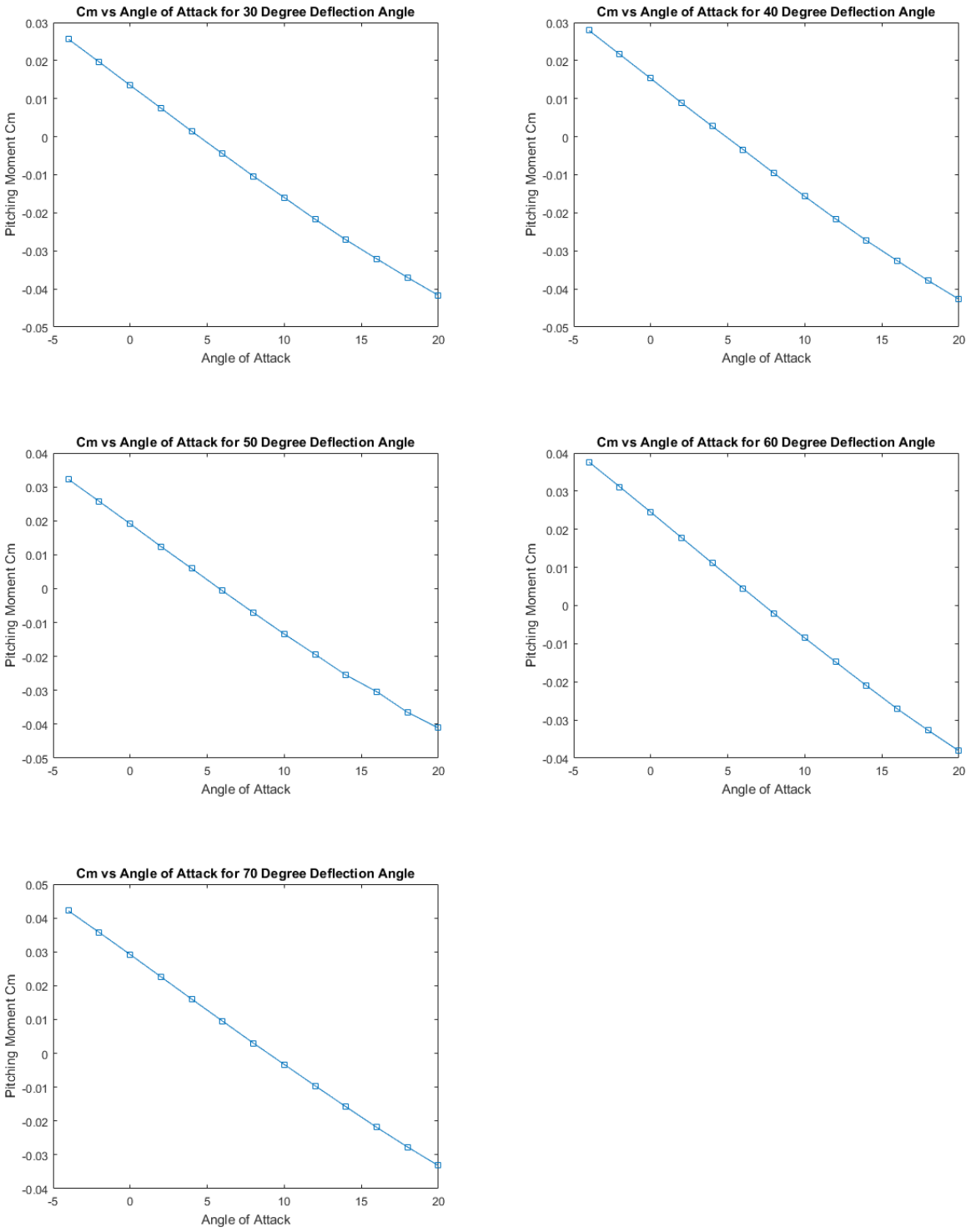

Figure 15: Pitching Moment Coefficients as a Function of Angle of Attack for Varying Flap Deflection Angles

The pitching moment coefficients ranged from positive values to negative values in all cases. Thus, a zero crossing exists and each deflection angle is capable of producing a trimmed vehicle. By interpolating each plot above to solve for the angle of attack at which the vehicle is trimmed, the following Figure 18 was produced.

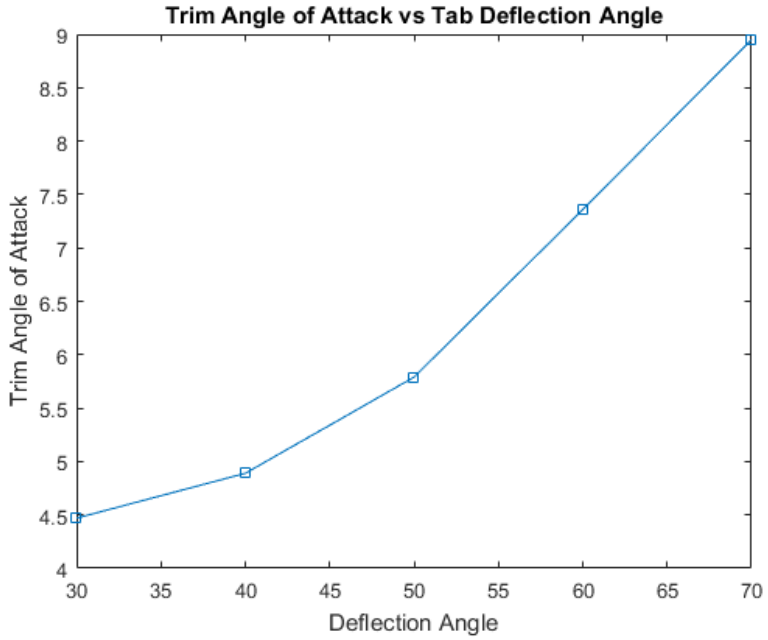

Figure 16: Trim Angle of Attack vs Flap Deflection Angle

The vehicle trims at higher angles of attack for larger flap deflection angles. This is expected due to the moment generated by the aerodynamic forces on the flap and the vehicle being symmetric. As the deflection angle approaches zero, the flap will no longer be in the flow so the trim angle of attack should also approach zero. Using the values for angle of attack at each flap deflection angle, the lift and drag coefficients were calculated. The plot for the trim lift coefficient is displayed in Figure 17.

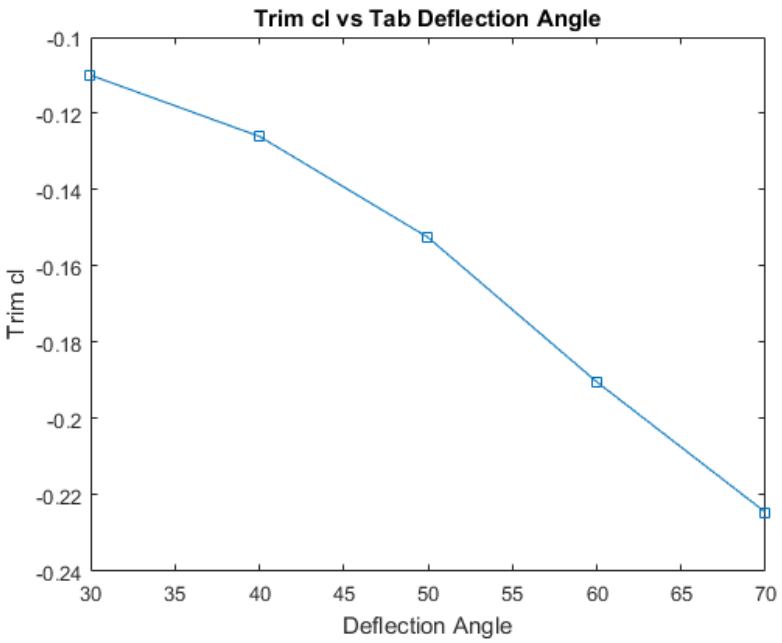

Figure 17: Trim Lift Coefficient vs Flap Deflection Angle

The lift coefficient increases and the flap deflection angle increases. The hinge effects are not modeled so that may also contribute to small parameter differences from the true value. The trend for a linear increase in flap deflection angle appears almost linear for trim c_l as well. Using the results from Figure 16, the trim drag coefficient was interpolated and plotted in Figure 18.

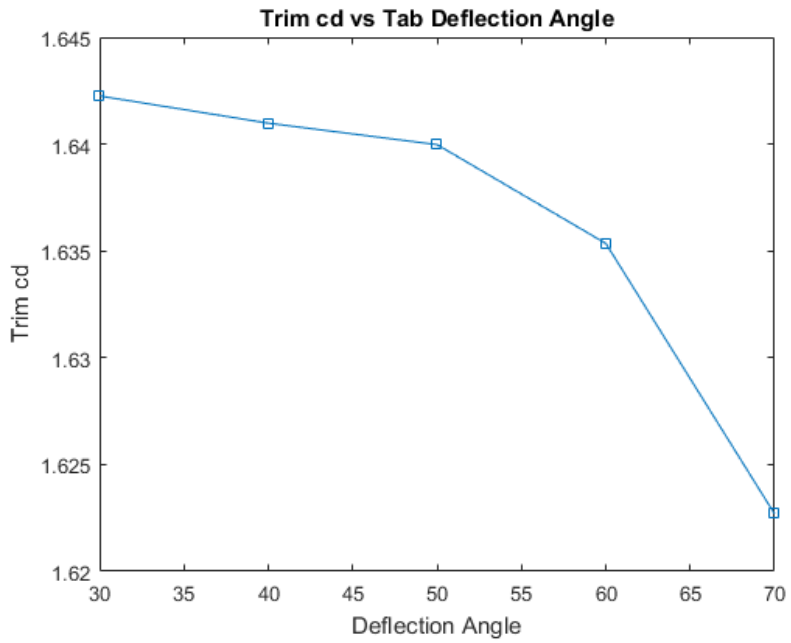

Figure 18: Trim Drag Coefficient vs Flap Deflection Angle

As the flap deflection angles increase, the value of the trim c_d decreases. The trend for this parameter is more exponential, different from what was observed in the trim c_l plot. As stated before, the lack of modeling of a flap hinge could contribute to discrepancies in this result from its true value. The trim lift-to-drag ratio was calculated by dividing the trim c_l and trim c_d for each deflection angle. Figure 19 displays L/D as a function of flap deflection angle.

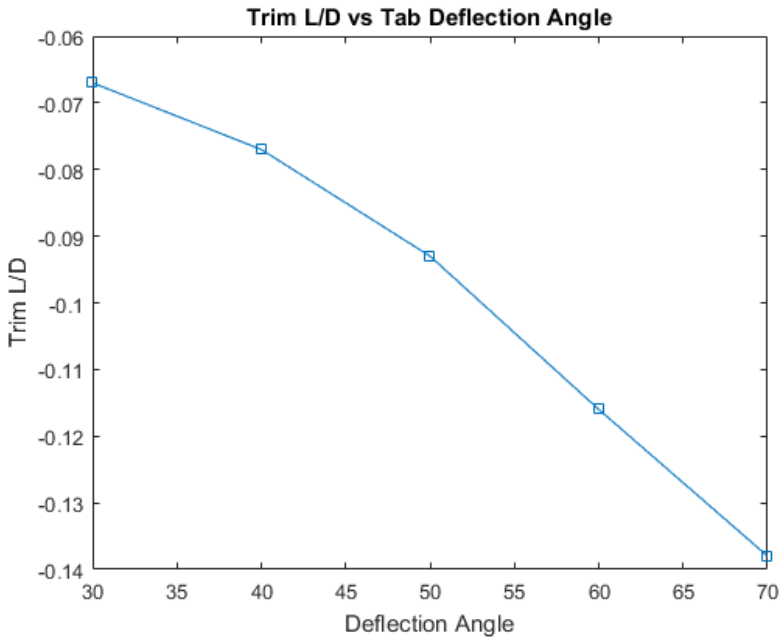

Figure 19: Trim Lift-to-Drag Ratio vs Flap Deflection Angle

This plot corresponds to the previous trim angle of attack plot in Figure 16 because larger trim angles of attack produce a larger trim L/D. It is shown that larger flap deflection angles produce a higher lift coefficient and lower drag coefficient. In this simulation, transient aerodynamic effects were neglected. However, it can be observed that the flap system has a significant impact on the vehicle's aerodynamic performance.

CHAPTER 5: CONCLUSION

The aerodynamic performance for various flap configurations on an entry vehicle was assessed in the hypersonic regime using a modified-Newtonian aerodynamic solution. Aerodynamic flaps directly control the lift vector using the vehicle's angle of attack and the flap drag area. This capability reduces the usage of the RCS jets, increasing the allowable payload mass, as well as mitigating RCS-jet-wake flow interaction effects. A constant attitude during descent combined with science instruments and sensors allows the entry vehicle to become a stable scientific platform exploring the atmospheric regime. Onboard terrain-matching sensors, such as radar, can enhance landing precision and accuracy, resulting in an increased mass delivery to higher elevation landing sites [10]. The implementation of flaps on an entry vehicle requires developing a mechanical actuation and deployment system, determining feasible vehicle configurations, performing aerothermodynamic analyses, identifying additional TPS capabilities, and identifying candidate GNC systems. The feasibility of using flaps as a viable method rather than bank-angle modulation depends on whether similar aerodynamic performance can be achieved.

The results presented demonstrate the effects of a flap on the aerodynamic performance of an entry vehicle during the hypersonic regime. A comparison of simulation and wind tunnel experimental results for a 70-degree sphere-cone with a vertical flap at 3% of the relative base area and located on top of the vehicle were shown as a validation case. The trim drag coefficients matched within eight percent at the maximum difference, while the trim lift coefficients matched within one percent. The trim angle of attack values were within 1.2 percent and the trim L/D values were within 7.4 percent for the two methods. Simulations for the same flap on a 70-degree sphere-cone deflecting from 30 degrees to 70 degrees relative to the vehicle's body axis were also conducted.

Results showed a decrease in trim drag coefficient, but an increase in trim lift coefficient, trim L/D, and trim angle of attack as the flap deflection angle increased. Simulations accounting for various vehicle configurations, defined by the quantity and size of each flap, can now be performed under various conditions since the method has been validated. The data acquired will allow for the creation of an aerodynamic database used to inform the development of entry vehicle configurations and guidance, navigation, and control systems to assess the system-level costs and benefits of flap-based hypersonic steering systems.

REFERENCES

[1] Kluever, C. A, "Entry Guidance Performance for Mars Precision Landing." *Journal of Guidance, Control, and Dynamics*. Vol. 31, No. 6, 2008, pp. 1537–1544.

[2] Mendeck, G. F. and Craig, L., "Mars Science Laboratory Entry Guidance." NASA, Houston.

[3] Putnam, Z and Braun, R., "Advances in Guidance, Navigation, and Control for Planetary Entry, Descent, and Landing Systems." *AAS Rocky Mountain Section Guidance and Control Conference*. Breckenridge, CO, 2016.

[4] Putnam, Z.R., "Improved Analytical Methods for Assessment of Hypersonic Drag-Modulation Trajectory Control," *Ph.D. Dissertation*, Georgia Institute of Technology, Atlanta, GA, 2015.

[5] Liang, Z, et al., "Optimal Bank Reversal for High-Lifting Reentry Vehicles." *IEEE Conference on Decision and Control*. Los Angeles, CA, 2014.

[6] Mendeck, G. F and Carman, G. L., "Guidance Design for Mars Smart Landers Using the Entry Terminal Point Controller." *AIAA Atmospheric Flight Mechanics Conference and Exhibit*. Monterey, CA, 2002.

[7] Horvath, T. J, et al., "Experimental Hypersonic Aerodynamic Characteristics of the 2001 Mars Surveyor Precision Lander with Flap." *AIAA Atmospheric Flight Mechanics Conference and Exhibit*. Monterey, CA 2002.

[8] Andersen, B. M. and Whitmore, S. A., "Aerodynamic Control on a Lunar Return Capsule using Trim-Flaps." *AIAA Aerospace Sciences Meeting and Exhibit*, Reno, NV, 2007.

[9] "IXV – Intermediate Experimental Vehicle – Spacecraft & Satellites." Spaceflight101.com. 2016. [Online]. [Accessed 17 Oct 2016].

[10] Korzun, A. M., et al., "Supersonic Aerodynamic Characteristics of Blunt Body Trim Tab Configurations." *AIAA Applied Aerodynamics Conference*. San Diego, CA, 2013.

[11] Dyakonov, A. A., et al., "Aerodynamic Interference Due to MSL Reaction Control System." *AIAA Thermophysics Conference*. San Antonio, TX, 2009.

[12] Seiff, A. and Kirk, D. B., "Structure of the Atmosphere of Mars in Summer at Mid-Latitudes." *Journal of Geophysical Research*. Vol. 82, No. 28, 1977, pp. 4364–4378.

[13] Braun, R. D. and Manning, R. M., "Mars Exploration Entry, Descent, and Landing Challenges." *Journal of Spacecraft and Rockets*. Vol. 44, No. 2, 2007, pp. 310–323.

[14] Spencer, D. A., et al., "Mars Pathfinder Entry, Descent, and Landing Reconstruction." *Journal of Spacecraft and Rockets*. Vol. 36, No. 3, 1999, pp. 357–366.

[15] Morabito, D. D., "The Spacecraft Communications Blackout Problem Encountered during Passage or Entry of Planetary Atmospheres." *IPN Progress Report 42-150*. 2002.

[16] "Antennas - Mars Reconnaissance Orbiter." NASA JPL. [Online]. [Accessed 17 Oct 2016].

[17] Sandford, S. P., et al., " Ares and Beyond: Autonomous Aerial Platforms Provide a Unique Measurement Capability for Earth and Planetary Science." *AIAA "Unmanned Unlimited" Systems, Technologies, and Operations.* 2003.

[18] "Could This Become The First Mars Airplane." NASA. [Online]. [Accessed 17 Oct 2016].

[19] "MEPAG." NASA. [Online]. [Accessed 28 Sept 2016].

[20] "HiRISE - Mars Reconnaissance Orbiter." NASA JPL. [Online]. [Accessed 10 Oct 2016].

[21] Kinney, D. J., "CBAERO 4.1+ User's Manual." 2012.

[22] Edquist, K. T., et al., "Aerodynamics for the Mars Phoenix Entry Capsule." *Journal of Spacecraft and Rockets.* Vol. 48, No. 5, 2011, pp. 713–726.